Hindawi
International Journal of RF and Microwave Computer-Aided Engineering
Volume 2023, Article ID 6256889, 9 pages
https://doi.org/10.1155/2023/6256889

Research Article

Compact Millimeter-Wave Antenna Array with Low Sidelobe Level for Vital Sign Monitoring Application

Mengxue He,[1] **Jie Yun**,[1] **Boning Wang**,[2] **Xuning Zhang**,[2] **and Xin Liao**[3]

[1]*Affiliated Hospital of Chengdu University of Traditional Chinese Medicine, Chengdu 610075, China*
[2]*University of University of Electronic Science and Technology of China, Chengdu 611730, China*
[3]*Chengdu University of Traditional Chinese Medicine, Chengdu 610075, China*

Correspondence should be addressed to Jie Yun; yunjie711024@163.com

Received 18 May 2023; Revised 1 September 2023; Accepted 2 November 2023; Published 25 November 2023

Academic Editor: Ali Gharsallah

In this paper, an antenna array fed in series by a novel substrate-integrated waveguide (SIW) power divider is proposed for the millimeter-wave band vital sign monitoring application. The proposed antenna is printed on a single-layer substrate, with the advantages of low profile, low cost, and ease of fabrication. By branching microstrip lines alternatively at both edges of the SIW, an in-phase power divider is first constructed. Then, by appropriately adjusting the depth of microstrip branches into the SIW, the amplitude of the output power can be tuned to obtain the desired amplitude distribution. Patches are connected to the microstrip branches, respectively, and thus, a radiation pattern with a low sidelobe level is realized. More importantly, series patches can be cascaded to enhance the array gain without the additional feeding network. This leads to a compact configuration. Based on the proposed idea, a prototype is designed, implemented, and tested. The results indicate that the proposed array achieves a maximum gain of 17.8 dBi with a low sidelobe level of -25.5 dB. The attractive performance shows that the array is suitable for the millimeter-wave vital sign monitoring application.

1. Introduction

Tracking of the physiological states of people can enable change of lifestyle recommendations and examine the risk of diseases. Compared with the traditional ways to monitor vital signs that require involving body-attached instruments, remote vital sign monitoring (RVSM) via radio frequency signals is cost-effective and less intrusive. It has attracted wide attention of researchers in recent years [1–3].

The antenna is a crucial component that determines the quality of received signals. The interference from other people around will worsen the received signals in RVSM. The design of an appropriate antenna is a challenging and meaningful task for wireless health monitoring systems. Efficient antennas with low sidelobe level (SLL) are desirable to mitigate the interference of the side reflections. Figure 1 illustrates a typical situation where a low sidelobe antenna is required for vital sign detection of a person with two other patients lying nearby. Besides, vertical polarization is also demanded to reduce the ground effect.

Many works about the low SLL design have been reported for the past few years. In [4], an X-band patch array with a low sidelobe is presented. A microstrip feeding network with unequal series-parallel power dividers is utilized to drive the patch antennas to realize a low SLL of less than -20 dB. The large-scale microstrip feeding network will cause significant losses at the millimeter-wave (mmWave) band, and it makes the antenna not applicable at higher frequencies. In [5], a Ku-band series-fed patch antenna array is designed with a low sidelobe. The authors proposed a differential evolution algorithm that uses two variables, element spacing and excitation amplitude, to further optimize the SLL. However, this antenna array has a narrow band. In [6], a series-fed patch antenna array is designed with unequal element spacing. The optimized array realizes a low SLL of -25.3 dB. An mmWave-band series-fed patch antenna array with a SLL of -25 dB is proposed in [7]. These series-fed patch arrays are restricted in the bandwidth and planar scalability. A series-fed binomial patch array with low sidelobe is reported in [8]. This work can realize an

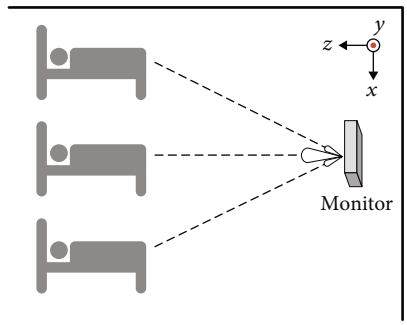

Figure 1: Situation of low SLL requirement in RVSM.

extremely low SLL down to -28 dB. But back feeding is required in this array, which is not suitable for planar integration. Some other microstrip-based linear arrays are proposed to realize the low sidelobe feature with a single-layer substrate [9, 10]. However, additional feeding networks will be required to realize the planar extension for these microstrip-based linear arrays. Thus, it is still a challenge to design a low sidelobe array printed on a single-layer substrate with high gain and compact size for the mmWave-band application.

In this paper, a vertically polarized patch antenna array fed by a novel substrate-integrated waveguide (SIW) feeding network is presented. By branching microstrip lines alternatively at both edges of the SIW and adjusting the depth of microstrip branches into the SIW, the desired amplitude distribution with identical phase is obtained at the output ports of the SIW feeding network. Low sidelobe radiation is achieved by connecting equally sized patches on the SIW. The feeding network arrays the elements in their H plane (x direction) to realize the vertical polarization (y direction), which differs from that in normal series-fed patch arrays [5, 7]. More interestingly, the designed SIW feeding network can be integrated between the antenna elements for compact size, and serial patches can be integrated on one port of the SIW for gain enhancement. The utilization of the feeding network simplifies array design and provides good scalability. The validation of the proposed antenna is conducted by implementation and measurement of an 18-element planar array. The antenna performance shows that our proposed array is suitable for the mmWave-band RVSM application.

2. Array Configuration

The configuration of the proposed array is shown in Figure 2. Parameter values are summarized in the caption. The antenna is printed on a Taconic RF-35 substrate with the thickness of 0.508 mm, relative dielectric constant ε_r of 3.5, and loss tangent δ of 0.0018. Additionally, the SIW is driven by a 50-Ω microstrip line for ease of integration. A tapered microstrip transition is used between the SIW and microstrip line for impedance matching and discontinuity reduction. The rectangular SIW is formed by installing three rows of metallized vias along the edges of a top copper patch. Besides, the metal ground coats the bottom of the substrate. The diameter (d) and spacing (s) of the vias can be optimized to maintain the conditions $d/s \geq 0.5$ and $d/\lambda_0 \leq 0.1$ (λ_0 is the free-space wavelength) to suppress the energy leakage [11].

Microstrip ports are alternatively introduced to both sides of the SIW with a periodic distance of $Da/2$ (about a half-guided wavelength λ_g), which ensures the in-phase excitation of radiation elements. The SIW feeding network with 9 output ports is designed in this work. By adjusting the depth L_{in} of microstrip line into the SIW, the amplitude of output signals can be tuned, and thus, the desired amplitude distribution can be obtained. We utilize the patch antennas with identical length L_c and width W_c as the radiation elements. Arrays of two-element series patches are connected to the ports, respectively, to construct the proposed low sidelobe antenna. We select 24 GHz as the design frequency.

3. Low Sidelobe Antenna Array

3.1. Substrate-Integrated Waveguide Feeding Network. Figure 3 illustrates the configuration of the proposed SIW feeding network. A 50-Ω microstrip line is used to drive the waveguide to facilitate the planar integration. We employ a typical microstrip-to-SIW transition between two structures for reflection reduction. The SIW is terminated in the short end with a row of vias. Standing waves operate in the waveguide.

The resonant frequency of the SIW can be calculated using the following equation:

$$f_{\text{SIW}}^{\text{TE}_{mn0}} = \frac{c}{2\sqrt{\varepsilon_r}} \sqrt{\left(\frac{m}{L_{\text{SIW}}}\right)^2 + \left(\frac{n}{W_{\text{SIW}}}\right)^2}, \quad (1)$$

where L_{SIW} and W_{SIW} represent the length and width of the SIW, respectively, and TE_{mn0} denotes the driven mode in SIW. To enable the excitation of nine ports, the TE_{910} mode is selected as the operational mode. Note that the design frequency of the SIW cavity needs to be slightly higher than the desired frequency due to the introduction of microstrip branches. Based on (1), the length Ls and width Ws are optimized to ensure that the desired mode of the SIW can be driven at the operational frequency.

The electric field distribution of the feeding network is shown in Figure 4. The direction of the electric field reverses every half wavelength λ_g. As demonstrated in Figure 4, output ports are alternatively introduced to both sides of the SIW with the reversal of field to ensure that the in-phase currents are obtained at all ports. Besides, each port is connected with the SIW where the field resonates strongly.

To achieve a low sidelobe level in radiation patterns of the antenna array, a weighting design is implemented in the feeding network. The Taylor distribution [12] with a SLL of -25 dB is applied to the linear 9-way network, which ensures in-phase feeding with equal spacing ($D_b/2$). The calculated Taylor field distribution is presented in Table 1.

In this design, the depth L_{in} of the microstrip lines into the SIW is a crucial factor that determines the feeding amplitude to obtain the desired field distribution. We conduct a

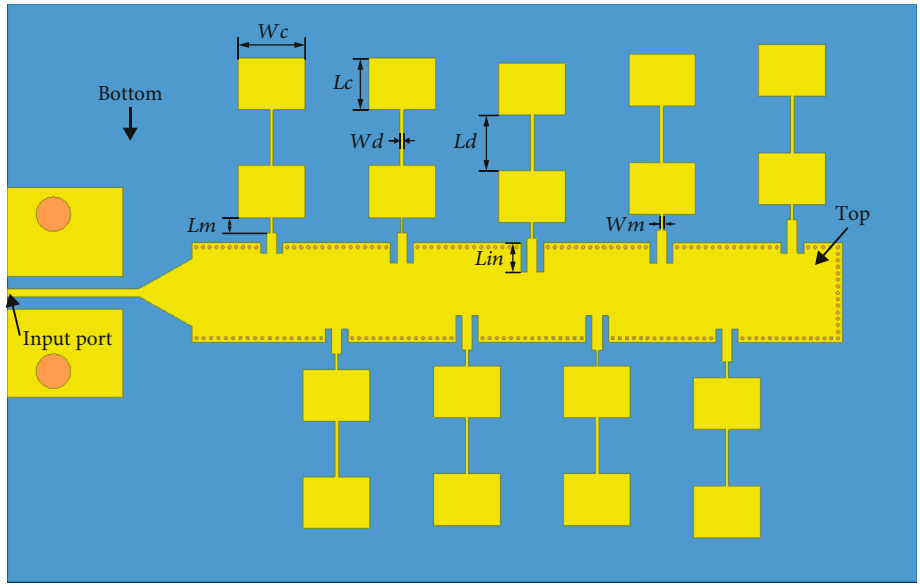

FIGURE 2: Configuration of the proposed array (Lm = 0.95, Wm = 0.15, Wd = 0.2, Ld = 3.4, Wc = 4.03, and Lc = 3.12 mm).

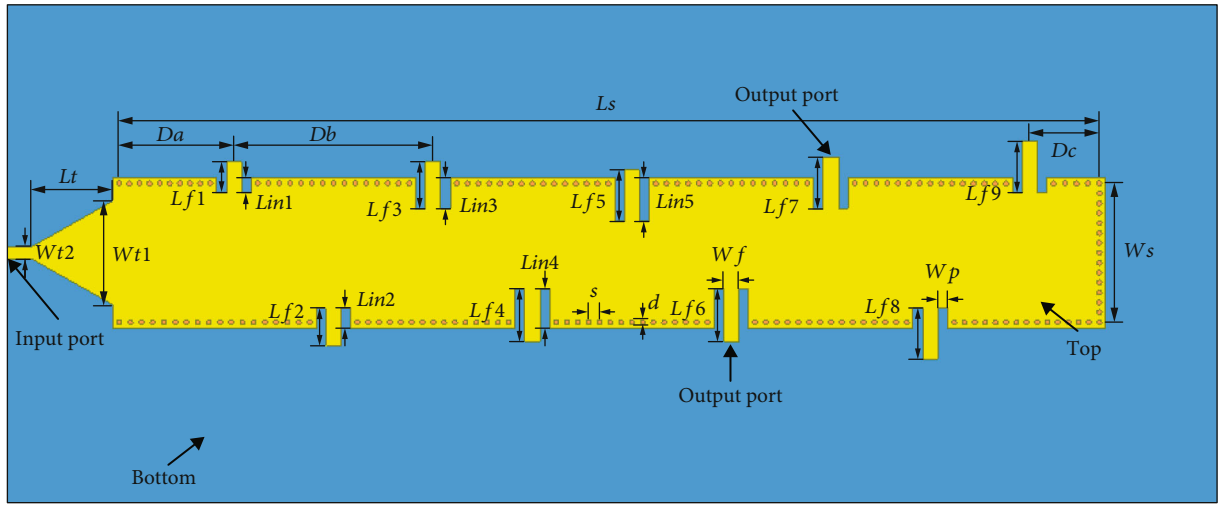

FIGURE 3: Configuration of the SIW feeding network (Wt1 = 4.1, Wt2 = 0.5, Lt = 3.19, Da = 4.8, Db = 7.88, Dc = 2.4, Ls = 39.3, Ws = 4.9, Wf = 0.6, $s = 0.4$, and $d = 0.2$ mm).

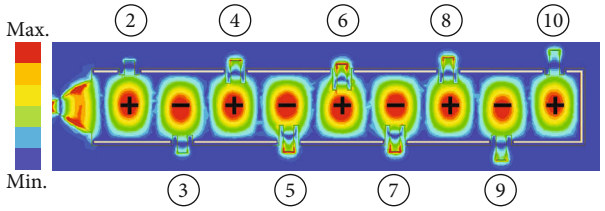

FIGURE 4: Electric field distribution of the feeding network.

parametric study of L_{in}. The simulated output power ratio with different lengths of L_{in} is plotted in Figure 5. As shown, the output power increases with the length of L_{in}. This feature can remain over a frequency band. It implies that the proposed array can achieve a stable radiation performance within the band. Besides, due to the variation of the depths L_{in}, the phase of the output signals will slightly fluctuate. Thus, the length of the microstrip branches Lf should be

TABLE 1: Comparison between the Taylor weight ratio and S parameters.

Ports	Taylor weight	S parameters	Normalized S parameters
2, 10	0.38	0.18	0.43
3, 9	0.53	0.23	0.56
4, 8	0.76	0.30	0.75
5, 7	0.94	0.37	0.91
6	1	0.41	1

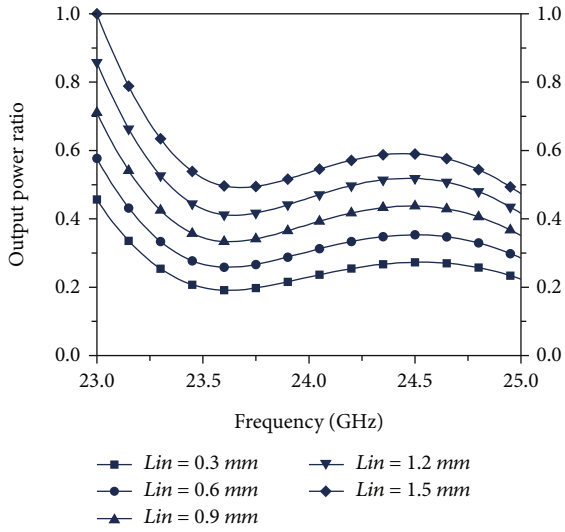

Figure 5: Simulated power ratio with different lengths of L_{in}.

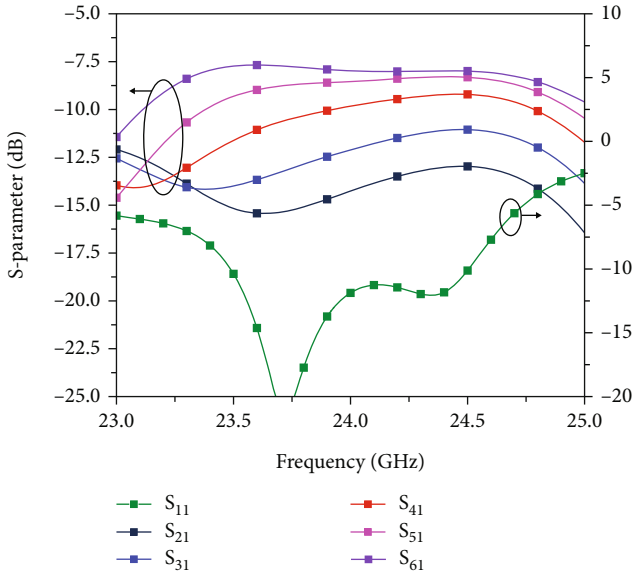

Figure 6: S parameter of the SIW feeding network.

finally optimized to obtain the in-phase output. The S parameter of the proposed feeding network is demonstrated in Figure 6. Due to the symmetric design, only the transmission coefficients of 5 ports are given in Figure 6. The optimized values of L_{in} and Lf with corresponding subscripts for 9 ports are summarized in Table 2. The S parameter values at the center frequency are given in Table 1. It is noted that the normalized values of the S parameters are in line with the calculated weight ratio.

Also, the location parameters Da and Db of the ports are important in the design of the feeding structure. A study is conducted to investigate these parameters, and the corresponding simulation results are presented in Figures 7 and 8. The distance Da between the first output port (port 2) and the transition structure mainly affects the impedance matching of feeding. As shown in

Table 2: Parameter values of L_{in} and Lf.

	2	3	4	5	6	7	8	9	10
L_{in}	0.62	0.8	1.24	1.59	1.77	1.59	1.24	0.8	0.62
Lf	0.6	0.7	0.6	0.5	0.3	0.5	0.8	1.2	1.4

Figure 7, the length of Da is optimized to 4.8 mm to achieve good matching. The distance between two adjacent ports on one side determines the feeding phase. Theoretically, a distance of one waveguide wavelength can result in in-phase feeding. In order to obtain the excitation with equal phase, the value of Db is optimized to 7.88 mm. With optimized values, the port phases of the feeding network are plotted in Figure 9. It can be seen that an acceptable phase difference of less than 40 degrees between ports is realized within the operation band of 23.5 GHz to 24.5 GHz. Besides, the parameter Dc should be designed to be approximately a quarter wavelength of the waveguide to ensure that the branches are located at the peak of the electric field.

3.2. Radiation Element and Array. In this work, patch antennas are utilized as the radiation elements for their advantages of stable patterns and ease of planar integration. Also, the patch antenna has vertically polarized radiation, which meets the requirement of the situation mentioned in Section 1.

According to the well-known cavity model theory [13], the patch antenna can be regarded as a resonant cavity surrounded by perfect magnetic conductor (PMC) boundaries, as depicted in Figure 10. The electric field distribution and resonant modes can be expressed in a similar manner to a resonant cavity.

$$E_z^{\mathrm{TM}_{mn}} = A_{mn} \cos \frac{m\pi x}{\mathrm{Lc}} \cos \frac{n\pi y}{\mathrm{Wc}}, \tag{2}$$

where Lc and Wc are the length and width of the patch antenna, respectively, and m, $n = 0, 1, 2, \cdots$. In higher order modes, alternate fields exist within the patch, leading to a reduction in radiation efficiency. Therefore, we select the fundamental mode TM_{10} as the operating mode for the patch. According to (2), the electric field distribution is illustrated in Figure 11. Due to the presence of the PHC boundaries, the electric field peaks occur at the edges of the patch, as shown in Figure 11.

Based on the cavity model theory, the resonant frequency of the patch antenna under TM_{10} mode can be expressed like a cavity as

$$f_{\mathrm{patch}}^{\mathrm{TM}_{10}} = \frac{c}{2\sqrt{\varepsilon_{\mathrm{eff}}}} \sqrt{\left(\frac{1}{L_{\mathrm{eff}}}\right)^2 + \left(\frac{0}{W_{\mathrm{eff}}}\right)^2}, \tag{3}$$

where $\varepsilon_{\mathrm{eff}}$ is the effective relative dielectric constant and L_{eff} and W_{eff} are the effective length and width of the patch, respectively. The calculation of these effective parameters can be referred to [14].

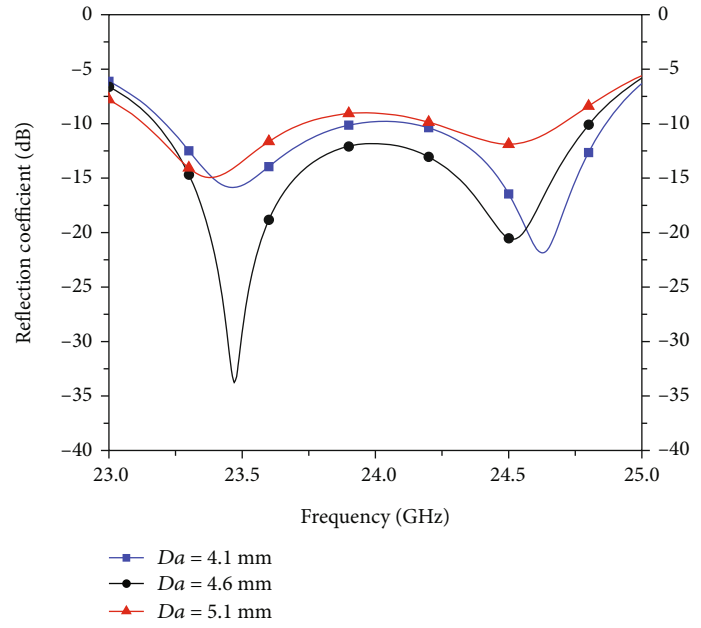

FIGURE 7: $|S_{11}|$ of the SIW feeding network with different values of Da.

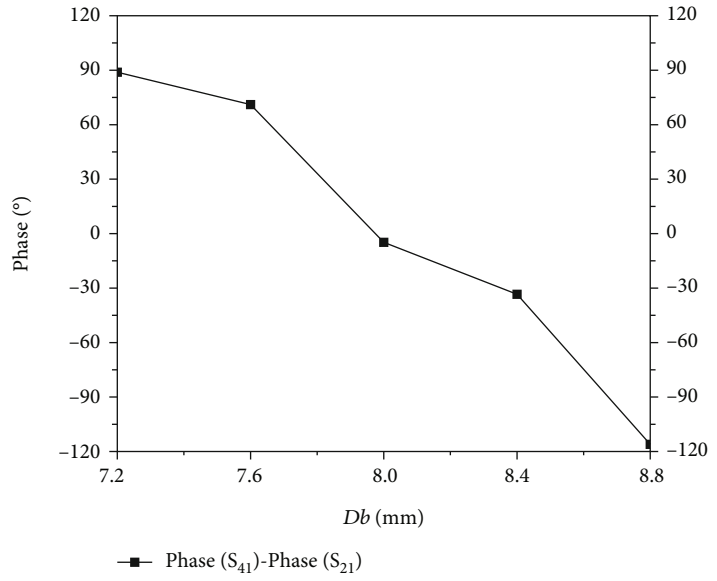

FIGURE 8: Phase difference between port 2 and port 4 with different values of Db.

In terms of radiation, the patch antenna can be considered as the operation of magnetic currents. According to the "Love's equivalence principle" [15], an equivalent current is generated along the periphery of the patch antenna, following its quasimagnetic wall. The current distribution can be analyzed using

$$\mathbf{M}_s = \mathbf{E} \times \hat{\mathbf{n}}. \tag{4}$$

where $\hat{\mathbf{n}}$ is the unit normal vector of the fictitious magnetic wall. Thus, in-phase currents are obtained at the wide sides (radiating sides) of the patch, while out-of-phase currents are present at the long sides (nonradiating sides).

To enhance the gain, we cascade two patch elements in a series connection to form a two-element antenna as the driven unit. More elements can be attached in series for higher gain. It indicates good scalability of this proposed array. The two-element antenna is designed and optimized separately. As shown in Figure 12, the length of the patch Lc determines the resonant frequency, and the value of 3.1 mm is selected for design. The fundamental mode TM_{10} of two elements are driven in phase and well matched with 70-Ω input impedance.

The proposed array is constructed by connecting the two-element antennas with the output ports of the SIW feeding network. The electric- (E-) field distribution of the

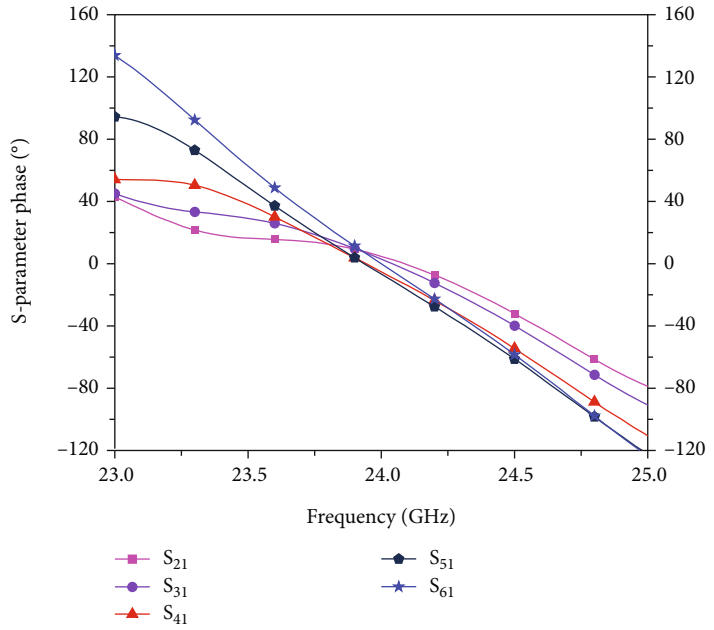

Figure 9: Port phases of the SIW network.

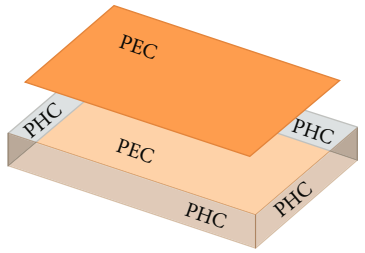

Figure 10: Cavity model of the patch antenna.

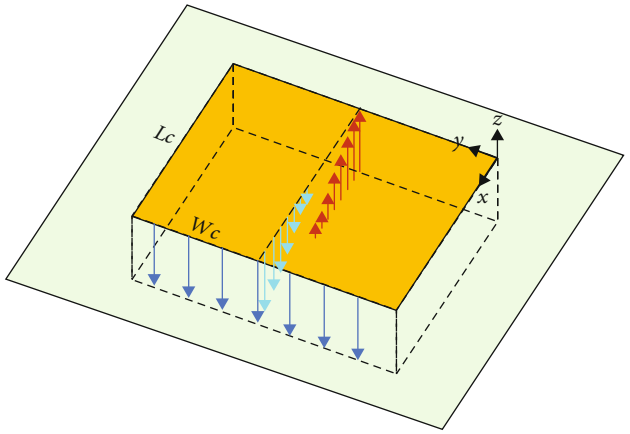

Figure 11: Electric field distribution of TM_{10} mode and equivalent magnetic currents.

array is illustrated in Figure 13. As expected, the distribution of the electric field on the array is tapered, which ensures the realization of low sidelobe.

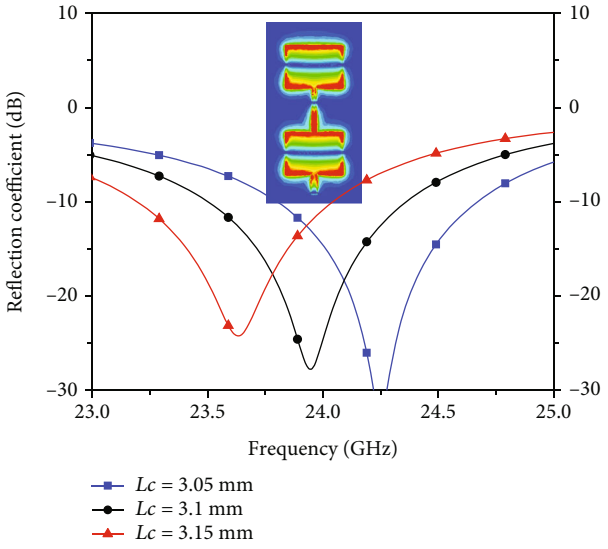

Figure 12: *S* parameter and E-field distribution of the two-element patch antenna.

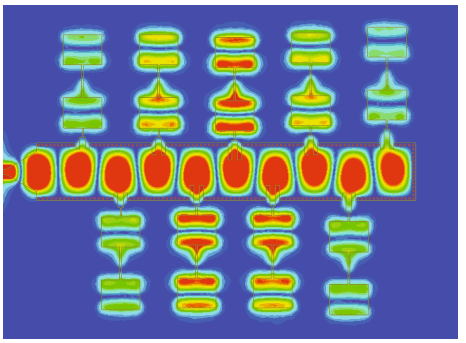

Figure 13: E-field distribution of the proposed array.

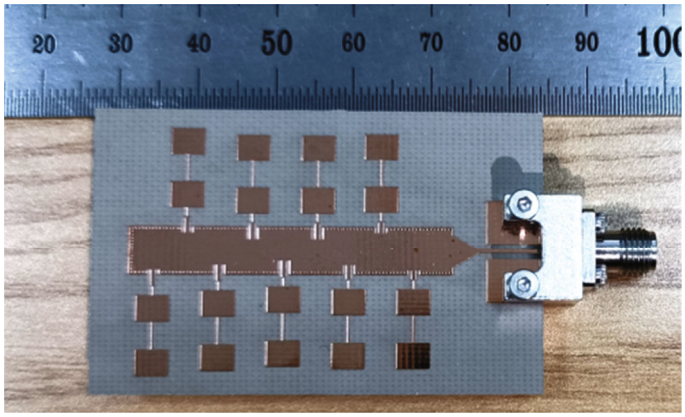

Figure 14: Photo of the fabricated prototype.

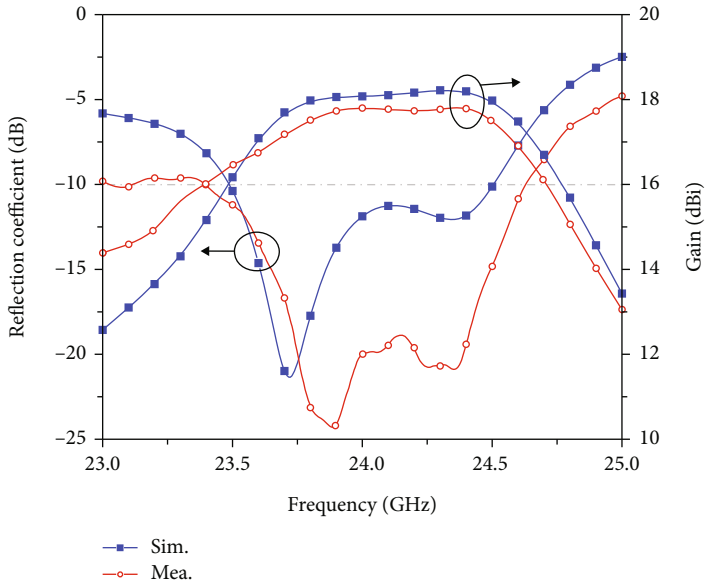

Figure 15: Results of the S parameter and broadside gain in simulation and measurement.

4. Implementation and Measurement

A prototype is fabricated and tested to verify the design method. The photo of the fabricated antenna is shown in Figure 14. The radiation performance of the antenna array is obtained by a far-field measurement system in an anechoic chamber. For the convenience of measurement, a high-frequency SMA connector is employed to connect the array with the test coaxial cable.

The measured and simulated results of $|S_{11}|$ parameter and broadside gain are compared in Figure 15. Based on the standard of $|S_{11}| < -10$ dB, the simulation and measurement results show a bandwidth of 23.49-24.51 GHz (4.25%) and 23.4-24.63 GHz (5.04%), respectively. The presence of two resonators, the SIW and patch antennas, in the array causes the appearance of two notched points on both curves. Besides, a maximum gain of 18.08 dBi and 17.8 dBi at 24 GHz is realized in simulated and measured results, respectively. The decreased measurement gain can be explained by losses that resulted from the test SMA connector.

Figure 16 shows the simulated and measured normalized copolarized radiation patterns of the SIW-fed array in its *xoz* plane. Owing to the standing-wave operation and in-phase excitation of the elements, broadside radiation is realized. A favorable agreement can be noticed in the main and side lobes of patterns between measured and simulated results. A favorable SLL of -25.5 dB in the H plane is achieved at 24 GHz according to the measurement. The SLL is suppressed to -18 dB and -24.2 dB at the lower and upper sideband, demonstrating a good sidelobe suppression effect. The measured results agree well with the simulated ones.

Finally, a comparison between the proposed array and previously reported single-layer low sidelobe arrays is conducted. The results are summarized in Table 3. Due to lack of the planar size of the substrate in most linear array articles, a comparison of aperture efficiency is not available.

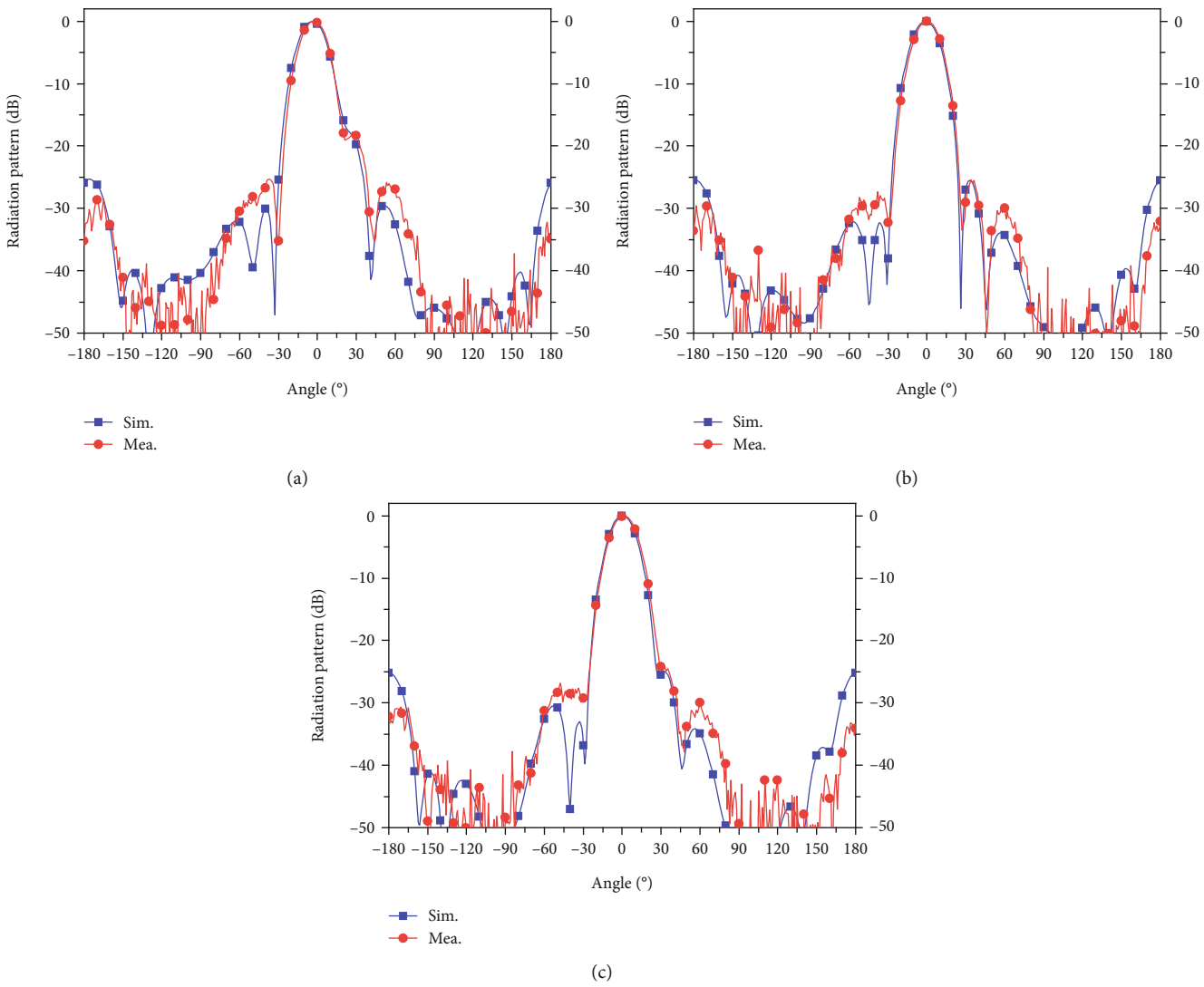

Figure 16: Simulated and measured radiation patterns of the proposed array at (a) 23.5 GHz, (b) 24 GHz, and (c)24.5 GHz.

Table 3: Comparison between proposed and reported single-layer low sidelobe arrays.

	Ref.			
	[7]	[9]	[16]	Our work
Center freq. (GHz)	24.125	79	24	24
Feeding lines	MS	MS	CPW + SIW	SIW + MS
Min. SLL (dB)	-24.7	-19.4	-22.5*	-25.5
# of element	1×26	1×18	4×32	$2 \times 4 + 2 \times 5$
Style of feeding	Back	Side	Back	Side
Impedance BW	1.04%	3.19%	1.7%	5%
Max. gain (dBi)	16.1*	13.88	24	17.8

MS: microstrip line; CPW: coplanar waveguide. *Obtained from the figure.

But the antenna efficiency can be roughly compared by the gain and element number. A higher gain with fewer elements implies that our proposed array will have a higher antenna efficiency. By utilizing the novel SIW feeding network, this work has developed outstanding performance in impedance bandwidth, antenna efficiency, and sidelobe level suppression, proving the validity of the array design method. Additionally, the presented method provides a good scalability for the array design.

5. Conclusion

An SIW-fed series patch antenna array with low sidelobe has been presented and implemented in this paper. A novel SIW feeding network with in-phase and unequal amplitude output is proposed. The short-ended feeding network operates in the standing-wave mode of TE_{10}. Microstrip ports are introduced alternatively to both sides of the feeding network to obtain the in-phase output power. More interestingly, by adjusting the depth of the microstrip ports into the SIW, the amplitude of the output power can be adjusted. Series patch antennas are cascaded to the microstrip ports to construct the high-gain planar array with low sidelobe.

Compared with the normal series-fed patch antenna, the proposed array has a wider bandwidth and favorable efficiency. More importantly, this array has a better scalability. Besides, results show a favorable agreement between simulation and measurement. This work provides a new and practical method for low-sidelobe-level array design in mmWave-band applications.

Data Availability

The data used to support the findings of this study are included within the article.

Conflicts of Interest

The authors declare that they have no conflicts of interest.

Acknowledgments

This work was supported by the Science and Technology Department of Sichuan Province under Grant 2022YFS0034.

References

[1] M. S. Rabbani and H. Ghafouri-Shiraz, "Frequency selective surface antenna for remote vital sign monitoring with ultra-wide band Doppler radar," *Microwave and Optical Technology Letters*, vol. 59, no. 4, pp. 818–823, 2017.

[2] T. Zhang, Z. Zhu, X. Ma, H. Xia, L. Li, and T. J. Cui, "A *W*-band integrated tapered array antenna with series feed for noncontact vital sign detection," *IEEE Transactions on Antennas and Propagation*, vol. 69, no. 6, pp. 3234–3243, 2021.

[3] Z. Xu, C. Shi, T. Zhang et al., "Simultaneous monitoring of multiple people's vital sign leveraging a single phased-MIMO radar," *IEEE Journal of Electromagnetics, RF and Microwaves in Medicine and Biology*, vol. 6, no. 3, pp. 311–320, 2022.

[4] S. X. Ta, V. D. Le, K. K. Nguyen, and C. Dao-Ngoc, "Planar circularly polarized X-band array antenna with low sidelobe and high aperture efficiency for small satellites," *International Journal of RF and Microwave Computer-Aided Engineering*, vol. 29, no. 11, Article ID e21914, 2019.

[5] T. Xu, M. Yao, F. Zhang, and X. Wang, "Design of low sidelobe series microstrip array antenna with non-uniform spacing and excitation amplitude," *Electronics Letters*, vol. 56, no. 21, pp. 1099–1101, 2020.

[6] J. Yin, Q. Wu, C. Yu, H. Wang, and W. Hong, "Low-sidelobe-level series-fed microstrip antenna array of unequal interelement spacing," *IEEE Antennas and Wireless Propagation Letters*, vol. 16, pp. 1695–1698, 2017.

[7] H. Khalili, K. Mohammadpour-Aghdam, S. Alamdar, and M. Mohammad-Taheri, "Low-cost series-fed microstrip antenna arrays with extremely low sidelobe levels," *IEEE Transactions on Antennas and Propagation*, vol. 66, no. 9, pp. 4606–4612, 2018.

[8] R. Chopra and G. Kumar, "Series-fed binomial microstrip arrays for extremely low sidelobe level," *IEEE Transactions on Antennas and Propagation*, vol. 67, no. 6, pp. 4275–4279, 2019.

[9] J.-I. Lee, J.-H. Lee, S.-H. Lee, and D.-W. Seo, "Low sidelobe design of microstrip comb-line array antenna using deformed radiating elements in the millimeter-wave band," *IEEE Transactions on Antennas and Propagation*, vol. 70, no. 10, pp. 9930–9935, 2022.

[10] J.-H. Lee, J. M. Lee, K. C. Hwang, D.-W. Seo, D. Shin, and C. Lee, "Capacitively coupled microstrip comb-line array antennas for millimeter-wave applications," *IEEE Antennas and Wireless Propagation Letters*, vol. 19, no. 8, pp. 1336–1339, 2020.

[11] M. Ali, K. K. Sharma, R. P. Yadav et al., "Design of dual mode wideband SIW slot antenna for 5G applications," *International Journal of RF and Microwave Computer-Aided Engineering*, vol. 30, no. 12, article e22449, 2020.

[12] C. A. Balanis, "Antenna synthesis and continuous sources," in *Antenna Theory: Analysis and Design, ch. 7*, pp. 406–416, John Wiley, Hoboken, NJ, USA, 3rd edition, 2005.

[13] P. Hammer, D. Van Bouchaute, D. Verschraeven, and A. Van de Capelle, "A model for calculating the radiation field of microstrip antennas," *IEEE Transactions on Antennas and Propagation*, vol. 27, no. 2, pp. 267–270, 1979.

[14] C. A. Balanis, "Microstrip antennas," in *Antenna Theory: Analysis and Design, ch. 14*, pp. 817–820, John Wiley, Hoboken, NJ, USA, 3rd edition, 2005.

[15] C. A. Balanis, "Aperture antennas," in *Antenna Theory: Analysis and Design, ch. 12*, pp. 653–673, John Wiley, Hoboken, NJ, USA, 3rd edition, 2005.

[16] J. Xu, Z. N. Chen, and X. Qing, "CPW center-fed single-layer SIW slot antenna array for automotive radars," *IEEE Transactions on Antennas and Propagation*, vol. 62, no. 9, pp. 4528–4536, 2014.